Korean J. Chem. Eng., 35(1), 110-117 (2018)
DOI: 10.1007/s11814-017-0278-8

pISSN: 0256-1115
eISSN: 1975-7220

CO_2 hydrogenation to methanol over Cu/ZnO catalysts synthesized via a facile solid-phase grinding process using oxalic acid

Wenze Li*, Peng Lu*,†, Ding Xu***, and Kai Tao**,†**

*School of Applied Chemistry, Shenyang University of Chemical Technology, Shenyang 110142, China
**Department of Materials, School of Materials Science & Chemical Engineering,
Ningbo University, Ningbo, Zhejiang 315211, China
***School of Biological and Chemical Engineering, Zhejiang University of Science and Technology, Hangzhou 310023, China
(*Received 20 July 2017 • accepted 2 October 2017*)

Abstract−Reduced Cu/ZnO catalyst was synthesized through solid phase grinding of the mixture of oxalic acid, copper nitrate and zinc nitrate, followed by subsequent calcination in N_2 atmosphere without further H_2 reduction. The catalysts were characterized by various techniques, such as XRD, TG-DTA, TPR and N_2O chemisorption. Characterization results suggested that during the calcination in N_2, as-ground precursor (oxalate complexes) decomposed to CuO and ZnO, releasing considerable amount of CO, which could be used for *in situ* reduction of CuO to Cu^0. The *in situ* reduced O/I-Cu/ZnO catalyst was evaluated in CO_2 hydrogenation to methanol, which exhibited superior catalytic performance to its counterpart O/H-Cu/ZnO catalyst obtained through conventional H_2 reduction. The decomposition of precursor and reduction of CuO happened simultaneously during the calcination in N_2, preventing the growth of active Cu^0 species and aggregation of catalyst particles, which was inevitable during conventional H_2 reduction process. This method is simple and solvent-free, opening a new route to prepare metallic catalysts without further reduction.

Keywords: CO_2 Hydrogenation, Methanol Synthesis, Solid Phase Grinding, Oxalic Acid, *In Situ* Reduction

INTRODUCTION

The continuous increase of atmospheric CO_2 concentration, the main greenhouse gas, has caused serious global warming and climate changes, threatening life on the earth. On the other hand, as a nontoxic, economical and renewable carbon resource, CO_2 is also a promising C1 building block for synthesizing various chemicals and carbonhydrates. Therefore, the utilization of CO_2 as carbon feedstock for producing transportation fuels and chemical feedstocks has recently aroused much attention worldwide [1-3]. Especially, the catalytic hydrogenation of CO_2 to methanol is believed to be an effective way of rational utilization of CO_2 [4-6]. This process has become a new research direction of methanol synthesis, attracting extensive attention from both fundamental and applied research [4].

However, it is very difficult to activate CO_2, considering its chemical inertness. Thus, CO_2 conversion is low in most hydrogenation reactions. The key to improving the activity of CO_2 hydrogenation is to explore highly active catalysts as well as novel reactors and process technology. Although many kinds of metal-based catalysts have been investigated for CO_2 hydrogenation to methanol, the most commonly used catalysts are the modified methanol catalyst for CO hydrogenation, such as supported Pd and Cu based catalysts [2-9]. The supported Pd catalysts exhibited considerable hydrogenation activity and selectivity to methanol [4]. However, the high price and scarcity of noble metal impedes their large-scale applications in industry. Alternatively, Cu-based catalysts with superior catalytic performance and low cost have been extensively studied for methanol synthesis reaction. Cu and Zn are the main components of classic catalysts used in industry for the synthesis of methanol from syngas (H_2/CO/CO_2). However, in the case of CO_2 hydrogenation to methanol, the yield of methanol over conventional methanol catalyst has been much lower than that obtained from syngas under similar reaction conditions [5]. Therefore, it is necessary to further improve the catalytic performance of Cu/ZnO catalyst to achieve satisfactory methanol yield for CO_2 hydrogenation.

It has been reported that catalytic performance of supported catalyst is sensitive to many variables, such as the nature of the support, promoters and catalyst preparation method. Different catalyst preparation methods could bring considerable variations in the structure of the precursors and final catalysts, which have significant influence on catalytic performance. The traditional preparation methods for preparation of Cu-based methanol catalysts mainly include coprecipitation, impregnation, and sol-gel methods [8-13]. More recently, many novel preparation methods, like low-temperature combustion synthesis method and solid phase synthesis method, have been developed to prepare high performance metal-based catalysts for various reactions [14-16]. Zhang et al. prepared nickel-containing ordered mesoporous silica materials (Ni-SBA-15) by solid-state grinding method and applied the materials in the dry reforming of methane (DRM) [17]. The as-synthesized Ni-SBA-15 catalyst showed enhanced Ni-support interaction and superior catalytic performance when compared with Ni/SBA-15 prepared by impregnation method. A mesostructured

†To whom correspondence should be addressed.
E-mail: taokai@nbu.edu.cn, lvpeng0830@zust.edu.cn

nickel nanoparticles embedded carbon/silica composite catalyst was successfully prepared via a solid-liquid grinding route, which displayed enhanced catalytic performance in carbon dioxide reforming of methane [18]. During the pyrolysis of catalyst precursor, Ni^0 species were formed *in situ* needing no further reduction, which would simplify the preparation of catalyst. Tang et al. studied solid state preparation of NiO-CeO_2 mixed oxides catalyst for NO reduction [19]. Improved textual properties and enhanced interfacial interaction between nickel and ceria were found. Consequently, the obtained catalyst exhibited good activity in NO reduction by CO. A practical soft reactive grinding route based on dry oxalate-precursor was employed to prepare Cu/ZnO catalysts for steam reforming of methanol to produce hydrogen [20]. The grinding-derived catalyst showed superior catalytic performance to the sample synthesized by coprecipitation method, owing to a higher Cu dispersion. Compared with wet-chemical method, the solid-phase synthesis route is simple and environmentally friendly, consuming less energy, which turns out to be a very promising strategy for fabricating high active catalysts for versatile reactions [15-20]. However, there are few reports on solid-phase synthesis of highly active Cu/ZnO for CO_2 hydrogenation to methanol. The influence of synthesis parameters on textural properties of as-obtained catalyst and corresponding catalytic performance has been insufficiently examined.

In this study, we prepared *in situ* reduced Cu-based catalysts by solid phase grinding method using oxalic acid as a chelating agent followed by calcination in N_2, and applied to the methanol synthesis reactions from CO_2 hydrogenation. The effects of catalyst synthesis parameters including oxalic acid dosage, calcination temperature, heating rate and holding time on the performances of the catalysts were systematically studied. The optimal catalyst exhibited a better catalytic performance than its counterpart catalyst, which was obtained through a conventional H_2 reduction, indicating the advantage of this *in situ* reduction method.

EXPERIMENTAL

1. Chemicals

Copper nitrate trihydrate ($Cu(NO_3)_2{\cdot}3H_2O$, 98%, AR), zinc nitrate hexahydrate ($Zn(NO_3){\cdot}6H_2O$, 99%, AR), and oxalic acid ($H_2C_2O_4$, 99%, AR) were purchased from Sinopharm Chemical Reagent Co., Ltd. All the chemicals were used without further purification.

2. Preparation of Catalysts

The Cu-based catalysts were prepared through solid phase grinding method using oxalic acid as a chelating agent at room temperature. Typically, $Cu(NO_3)_2{\cdot}3H_2O$, $Zn(NO_3)_2{\cdot}6H_2O$ (Cu/Zn mole ratio of 1/1) and a certain amount of oxalic acid were physically mixed in an agate mortar, and then manually ground for 0.5 h at room temperature. The obtained light blue precursor (metal complexes) was dried at 393 K for 12 h, and then calcined at 623 K for 3 h in N_2 flow with ramping rate of 3 $K{\cdot}min^{-1}$, followed by passivation in 1% O_2/N_2 flow for 5 h at room temperature. The catalyst was *in situ* reduced without further reduction and denoted as O/I-Cu/ZnO. To compare the influence of the reduction method on the catalyst performance, a control catalyst with conventional H_2 reduction was also prepared by following steps: (i) calcining the dried precursor at 623 K for 3 h in air, (ii) reducing the oxide at 503 K for 10 h in 5% H_2/N_2 flow, and (iii) passivating the catalyst in 1% O_2/N_2 flow at room temperature for 5 h. The control catalyst was marked as O/H-Cu/ZnO.

3. Characterization of Catalysts

The phase structures of the samples were analyzed by X-ray diffractometer (XRD, Bruker D8 Advance) using monochromatic Cu-Kα radiation in the scanning 2θ angle range from 20 to 80°, operated at 40 kV and 40 mA. The specific surface area, pore volume and adsorption-desorption isotherms of the catalysts were measured by a physical adsorption analyzer (Autosorb-iQ-C). The thermal behavior of samples was analyzed by thermogravimetric analysis (TG-DSC) using a NETZSCH thermoanalyzer (model STA 449F3). The surface morphology of samples was observed using scanning electron microscopy (SEM, JSM-6360LV) equipped with an energy-diffusive X-ray spectroscopy (EDX).

Temperature programmed reduction (H_2-TPR) experiments were performed on a Belcat-B3 automatic chemical adsorption instrument. In each run, 0.2 of catalyst was loaded at the center of a U-shaped quartz reactor (i.d. 6 mm). The sample was first purged with Ar at 323 K for 2 h, followed by cooling to room temperature. Then, a 10% H_2/Ar (20 $ml{\cdot}min^{-1}$) flow was passed over the sample, and the temperature was linearly raised from 298 to 700 K with a heating rate of 10 $K{\cdot}min^{-1}$. The H_2 consumption was detected by a thermal conductivity detector (TCD).

N_2O pulse chemisorption was performed to determine the active metallic copper (Cu^0) surface area. 0.2 g of sample was placed in a quartz tube reactor and the temperature was raised to 363 K under helium atmosphere. A pulse of N_2O was passed over the catalyst. N_2O can oxidize Cu^0 to Cu_2O phase. By quantifying the total amount of consumed N_2O of all pulses, the Cu^0 surface area of the catalyst can be calculated [12].

4. Catalytic Activity Measurements

The catalytic hydrogenation of CO_2 to methanol was performed in a continuous-flow fixed-bed stainless steel tubular reactor. In each test, 0.5 g of catalyst was placed at the center of the reactor and sandwiched by quartz wool. The liquid product was collected by a cold trap, where 25 ml of 2-butanol of was added. The reactor was purged by the feed gas ($Ar/CO_2/H_2$=3/25/72) before the pressure was elevated to 3.0 MPa at 298 K. The reaction was conducted at 523 K with a total flow rate of 18 $ml{\cdot}min^{-1}$. The gas products were analyzed by an online GC equipped with a TCD and a TDX-01 column, and the liquid products were analyzed by an offline GC equipped with a flame ionization detector (FID) and a RESTEK Rtx-5 capillary column.

RESULTS AND DISCUSSION

1. XRD Analysis

The Cu/ZnO catalyst was obtained by grinding starting materials followed by calcination in N_2. To reveal the evolution of catalyst phase structure, XRD patterns of dried precursor as well as calcined catalysts obtained in air or N_2 atmosphere were collected and compared in Fig. 1. As shown in Fig. 1(a), two main diffraction peaks appeared at 22.8 and 24.3°, which could be ascribed to copper oxalate and zinc oxalate phase, respectively [20,21]. There is no characteristic diffraction peak related to Cu^0, CuO or ZnO

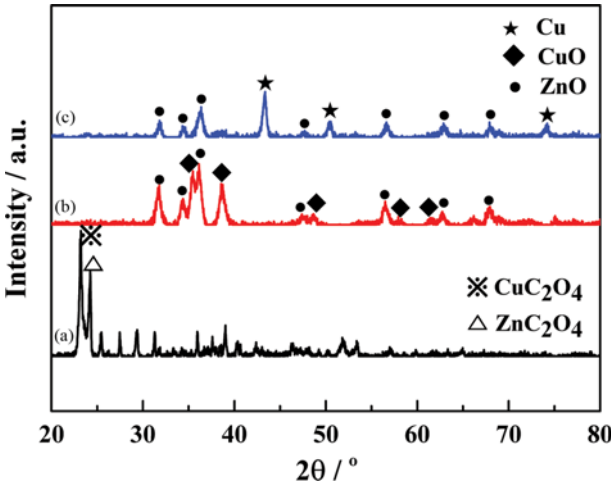

Fig. 1. XRD patterns of dried precursor (a), calcined catalyst in air (b) and calcined catalyst in N_2 (c).

observed, suggesting that only oxalate complexes were formed during the solid phase grinding process. The XRD pattern (Fig. 1(b)) significantly changed when the precursor was calcined in air. The peaks at 35.5°, 38.7°, 48.8°, 58.2° and 61.5° were assigned to CuO phase [14], and the peaks at 31.2°, 34.4°, 36.3°, 47.5°, 56.7°, 62.9° and 68.0° to ZnO phase [20]. No other impurity diffraction peaks are observed in Fig. 1(b), which indicates that the oxalate precursors decomposed completely to CuO and ZnO after calcining in air. As for the sample calcined in N_2, the XRD pattern (Fig. 1(c)) displays diffraction peaks of ZnO (31.2°, 34.4°, 36.3°, 47.5°, 56.7°, 62.9° and 68.0°). However, the diffraction peaks of CuO disappeared and the characteristic peaks of Cu^0 (43.2°, 50.4° and 74.5°) [14,20] appeared when compared to the sample calcined in air. It is inferred that the precursor was first decomposed to generate CuO and ZnO (Eqs. (1) and (2)), and the CuO was then *in-situ* reduced to Cu^0 (Eq. (3)) by the CO (see below) generated during the calcination [22-24]. When the oxalate precursor was heated in N_2, the decomposition and reduction of the precursor proceeded simultaneously to produce the final catalyst. Therefore, reduced Cu/ZnO catalyst could be successfully prepared by grinding corresponding oxalates followed by calcination in N_2.

$$CuC_2O_4=CuO+CO+CO_2 \quad (1)$$

$$ZnC_2O_4=ZnO+CO+CO_2 \quad (2)$$

$$CO+CuO=Cu+CO_2 \quad (3)$$

To understand the dependence of catalyst structure on the ratio of oxalic acid to metal nitrates, XRD patterns were collected and the results are presented in Fig. 2. For the catalyst synthesized without oxalic acid (Fig. 2(a)), only diffraction peaks of the CuO and ZnO are observed, indicating the decomposition of nitrates to CuO and ZnO. With the addition of oxalic acid, the characteristic diffraction peaks Cu^0 appeared as shown in Fig. 2(b)-(i). With increase of $(COOH)_2$/(Cu+Zn) ratio from 0.5/1 to 3.5/1, the intensity of Cu^0 diffraction peaks continuously increased. Further increasing the $(COOH)_2$/(Cu+Zn) ratio (Fig. 2(g)-(i)), the intensity of Cu^0 diffraction peaks slightly changed and the diffraction peaks

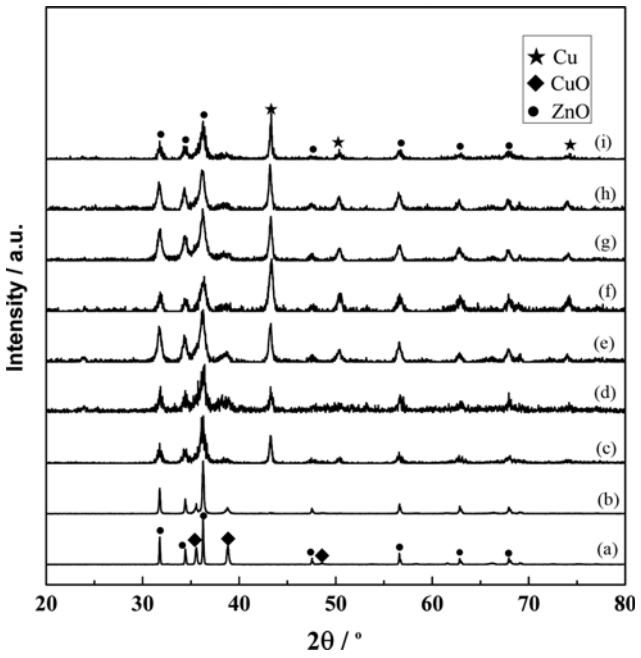

Fig. 2. XRD patterns of Cu/ZnO catalysts prepared by grinding method after calcination in N_2 at various $(COOH)_2$/(Cu+Zn) ratio: (a) 0/1, (b) 0.5/1, (c) 1/1, (d) 2/1, (e) 3/1, (f) 3.5/1, (g) 4/1, (h) 5/1 and (i) 6/1.

corresponding to CuO almost disappeared. When the amount of oxalic acid was low (Fig. 2(b)-(e)), the nitrates could not be totally converted to oxalates. So, the CO generated was insufficient to reduce all the CuO formed during the decomposition process of the as-ground precursor in N_2. Thus, the catalyst was composed of Cu^0 and CuO species. At appropriate $(COOH)_2$/(Cu+Zn) ratio (>3/1), the released CO could ensure the full reduction of Cu^{2+} to

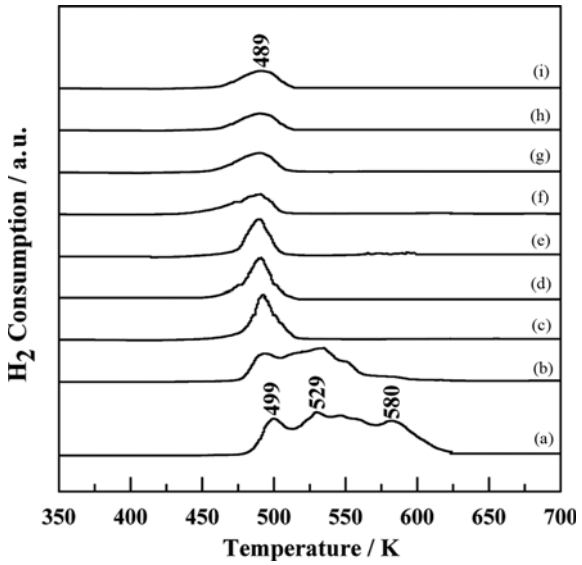

Fig. 3. H_2-TPR profiles of Cu/ZnO catalysts prepared by grinding method after calcination in N_2 at various $(COOH)_2$/(Cu+Zn) ratio: (a) 0/1, (b) 0.5/1, (c) 1/1, (d) 2/1, (e) 3/1, (f) 3.5/1, (g) 4/1, (h) 5/1 and (i) 6/1.

Cu^0. Therefore, *in situ* reduced Cu/ZnO catalyst could be successfully synthesized by the solid phase grinding method followed by calcination in N_2 atmosphere when the $(COOH)_2$/(Cu+Zn) ratio larger than 3.

2. H_2-TPR Analysis

The effect of $(COOH)_2$/(Cu+Zn) ratio on the reducibility of passivated catalysts was investigated by H_2-TPR (Fig. 3). As shown in Fig. 3(a), several overlapping reduction peaks in the temperature range of 480-624 K are observed for catalyst prepared without addition of oxalic acid. Three main reduction peaks at 499, 529 and 580 K can be ascribed to the different types of CuO phase, since ZnO cannot be reduced below 624 K [25-27]. The lower temperature peaks were attributed to the reduction of higher dispersed CuO species, and the higher temperature one was related to the reduction of bulk CuO [25-27]. Besides, the reduction profile was broad and asymmetrical, indicating a broad particle size distribution of CuO species [20]. Because there was no oxalic acid in the grinding process, the CuO and ZnO generated by nitrate decomposition were isolated from each other. So, the particle size was bigger and heterogeneous. As the amount of oxalic acid increased, the TPR reduction band gradually turned into a narrow single reduction peak. The reduction peaks shifted to lower temperatures and their intensities weakened with increasing $(COOH)_2$/(Cu+Zn) molar ratio from 0.5/1-3/1 (Fig. 3(b)-(e)). When $(COOH)_2$/(Cu+Zn) molar ratios were larger than 3/1, the catalysts showed similar reduction profile (Fig. 3(f)-(i)). As confirmed by XRD analysis in Fig. 2, the CuO cannot be fully reduced in the calcining process of the as-ground precursor when the $(COOH)_2$/(Cu+Zn) molar ratio is smaller than 3/1, resulting in the coexistence of CuO and Cu^0, since the amount of oxalic acid was insufficient in the as-ground precursor. Therefore, the reduction band in for Fig. 3(b)-(e) could be attributed to the reduction of residual CuO during the catalyst preparation and the CuO film formed by re-oxidation of Cu^0 after the passivation with diluted O_2. When the amount of oxalic acid was sufficient ($(COOH)_2$/(Cu+Zn)>3.5/1), the generated CuO could be completely reduced during calcination process. So, the single reduction peak (Fig. 3(f)-(i)) was solely related to the CuO film formed during the passivation process, owing to the re-oxidation of *in-situ* generated Cu^0 during the preparation of catalyst. The TPR result was in good agreement with XRD.

3. TG-DSC Analysis

The thermal decomposition behavior of oxalic acid and the as-ground oxalates precursor was studied by TG-DSC (Fig. 4). A first weight loss of 27.6 wt% at 323-410 K (Fig. 4(a)) accompanied with an endothermic peak centered at 384 K (Fig. 4(c)) are observed, which was attributed to the dehydration of oxalic acid. The second weight loss of 72.4 wt% in the temperature range of 410-480 K, characterized by a sharp endothermic peak at 472 K, was caused by the decomposition of oxalic acid [22]. For the as-ground oxalates precursor, the first two weight loss peaks could be attributed to the dehydration and decomposition of excess oxalic acid, respectively. Moreover, two weight losses accompanied by two corresponding exothermic peaks were observed at temperature ranging from 570 to 680 K, which could be assigned to the decomposition of CuC_2O_4 in the precursor to form of CuO-ZnC_2O_4 mixture and the further decomposition of ZnC_2O_4 to produce CuO-ZnO [20-24]. Note that although the decomposition reactions of the CuC_2O_4 and ZnC_2O_4 were endothermic, exothermic peaks existed on DSC curves caused by the exothermic air oxidation of CO to CO_2 ($2CO+O_2 \rightarrow 2CO_2$), which was usually observed in the thermal decom-

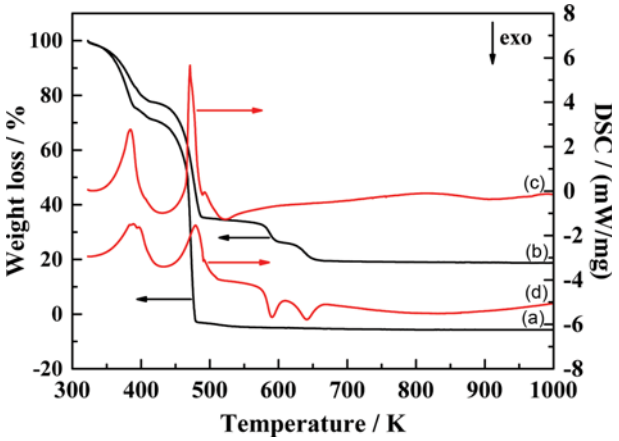

Fig. 4. TG-DSC curves of oxalic acid (a), (c) and as-ground oxalates precursor (b), (d) in air atmosphere.

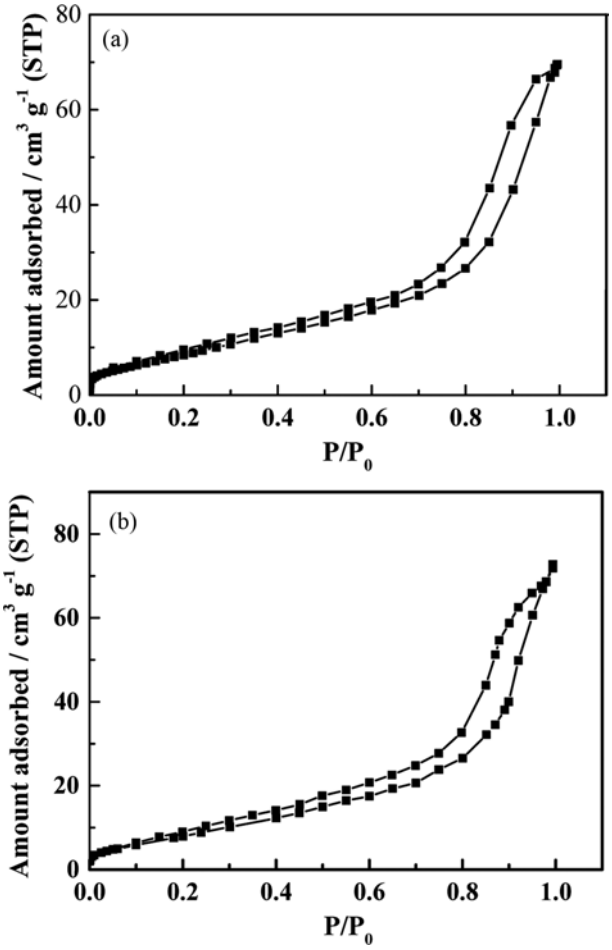

Fig. 5. N_2 adsorption-desorption isotherms of O/I-Cu/ZnO (a), and O/H-Cu/ZnO (b) catalysts.

Table 1. Specific surface area and pore parameters of catalysts

Catalyst	Surface area/ $m^2 \cdot g^{-1}$	Pore volume/ $ml \cdot g^{-1}$	Pore diameter/ nm
O/H-Cu/ZnO	32.97	0.11	3.82
O/I-Cu/ZnO	38.19	0.18	3.04

position of metal oxalate in air [22-24].

Combined with XRD and H_2-TPR analysis in Fig. 1 and Fig. 3, it is concluded that reduced O/I-Cu/ZnO catalyst can be successfully prepared through the decomposition of metal oxalates and following *in situ* reduction (Eq. (1)-(3)) under appropriate amount of oxalic acid/metal nitrates ratio (3.5/1).

4. Analysis of Pore Structure and Specific Surface Area

The adsorption-desorption isotherms of O/I-Cu/ZnO and O/H-Cu/ZnO catalyst are shown in Fig. 5. Both displayed typical type IV isotherms with H1-type hysteresis loops, which are characteristic of mesoporous materials [28]. The specific surface area calculated by the Brunauer-Emmett-Teller (BET) method, and the pore parameters measured by multiple Barrett-Joyner-Halenda (BJH) methods using adsorption branches of nitrogen adsorption-desorption isotherms are summarized in Table 1. Compared with O/I-Cu/ZnO, O/H-Cu/ZnO showed smaller BET surface area and pore volume. This was possibly due to particle aggregation and sintering, since a long time high temperature H_2 reduction process was required for O/H-Cu/ZnO catalyst.

5. Analysis of Surface Morphology

The surface morphologies of the dried precursor, O/I-Cu/ZnO and O/H-Cu/ZnO were observed by SEM, and the SEM images are shown in Fig. 6. There were several irregular particles, such as block, cylindrical and spherical in the dried precursor, and their size distribution was not uniform (Fig. 6(a)). It is indicated that the copper oxalate and zinc oxalate crystals with uneven distribution were generated by the solid phase reactions between metal nitrates with oxalic acid after grinding. For the *in situ* reduced O/I-Cu/ZnO catalyst obtained in N_2 atmosphere, there were some spherical particles with uniform size (200-300 nm) on the surface of catalyst as shown in Fig. 6(b). In contrast, for conventional H_2 reduced O/H-Cu/ZnO catalyst, many agglomerates were observed (Fig. 6(c)). The high temperature calcination in air and subsequent H_2 reduction resulted in the agglomeration of particles. So, the particle distribution was asymmetrical, and the average particle size was bigger than that of O/I-Cu/ZnO catalyst.

6. Catalyst Performances

6-1. Influences of Oxalic Acid Dosage on Catalyst Performances

Cu-based catalysts have been intensively explored for hydrogenation of CO_2 to methanol, even though the nature of the active site is yet to be fully understood. There are different points of view on the nature and valence of copper sites. Some studies suggest that Cu^+ sites are the active catalytic centers. For example, Sznyi et al. found that the activity for methanol synthesis on clean Cu (100) was lower than that on oxidized Cu (100), proving that the Cu ion was the active site [29]. Van Santen et al. suggested that the stabilization of Cu^+ could promote the activity of the methanol catalyst [30]. On the other hand, some researchers pointed out that metallic Cu was active for methanol synthesis. According to a recent work [31], the mechanism for CO_2 hydrogenation to methanol involves the adsorption of CO_2 on support (generating formate species) and the dissociative adsorption of H_2 on Cu surface. The dissociatively adsorbed H_2 then reacts with formate species to form methoxy species. Finally, the methoxy species is hydrogenated to methanol. Therefore, the numbers of exposed metallic Cu is crucial for the reaction. Many previous studies have suggested that the activity of the catalyst is directly proportional to the number of metallic Cu [32]. Further evidence supporting metallic Cu as the active site is provided by experiments on single crystal Cu(100), Cu(110), and polycrystalline Cu films exposing primarily Cu(111) facets [33-36]. In addition, a synergistic effect between the ZnO support and metal Cu particles may also contribute to activity [37], increasing the complexity of the reaction mechanism and the nature of its active site. In this study, the amount of oxalic acid has a significant influence on chemical states of Cu, and may affect the catalytic performance. The catalytic performance of O/I-Cu/ZnO catalysts prepared at various $(COOH)_2$/(Cu+Zn) molar ratios is presented in Table 2. It is observed that the CO_2 conversion, and the selectivity and yield to the methanol increased with the increase of $(COOH)_2$/(Cu+Zn) molar ratio from 0 to 3.5/1. Then, the CO_2 conversion, and the selectivity and yield to methanol decreased if the $(COOH)_2$/(Cu+Zn) molar ratio was continuously increased. When there is no oxalic acid or oxalic acid dosage is too little, the metal nitrates cannot be fully converted to oxalate complexes in the grinding reaction process, resulting in formation

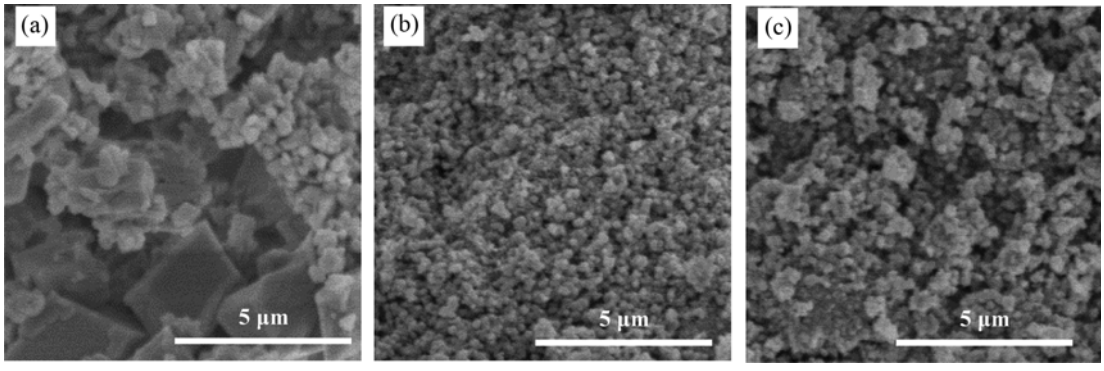

Fig. 6. SEM images of dried precursors (a) O/I-Cu/ZnO, (b) and O/H-Cu/ZnO (c).

Table 2. Influences of oxalic acid dosage on catalyst performances[a]

$(COOH)_2$/(Cu+Zn)	CO_2 conversion/%	Selectivity/%		CH_3OH yield/%	S_{BET}[b]/$m^2 \cdot g$	d_{Cu}[c]/nm
		CO	CH_3OH			
0/1	0.8	100	0	0	9.7	—
0.5/1	1.8	100	0	0	14.8	—
1/1	7.8	92.6	7.4	0.6	23.7	97.2
2/1	26.1	19.4	80.6	21.1	26.0	25.2
3/1	26.6	16.3	83.7	22.2	32.3	23.1
3.5/1	29.2	16.4	83.6	24.4	38.2	20.1
4/1	28.2	18.9	81.1	22.9	34.7	22.1
5/1	28.0	18.3	81.7	22.8	32.2	23.3
6/1	27.7	19.3	80.7	22.4	29.8	31.8

[a]Reaction conditions: 523 K; 3.0 MPa; catalyst weight: 0.5 g; $Ar/CO_2/H_2$=3/25/72; flowing rate: 18 $ml \cdot min^{-1}$; reaction time: 4 h
[b]BET specific surface area
[c]d_{Cu} determined by the XRD pattern based on Scherrer equation

of isolated CuO and ZnO after calcination in N_2. Therefore, the particles in the samples agglomerated and sintered easily, and specific surface area was low. Furthermore, the CuO cannot be reduced to Cu^0, if oxalic acid is not enough. There was no Cu^0 species in the samples obtained with $(COOH)_2$/(Cu+Zn) molar ratio of 0/1 and 0.5/1 as confirmed by XRD (Fig. 2(a)-(b)) and TPR (Fig. 3(a)-(b)). Thus, the catalysts showed no activity in the CO_2 hydrogenation to methanol. When the amount of oxalic acid was sufficient, the nitrates could be fully converted to zinc and copper oxalate complexes precursor, and the CuO could be reduced to Cu^0. Besides, the interacting ZnO improved the dispersion CuO and Cu^0. Therefore, as the $(COOH)_2$/(Cu+Zn) molar ratio increased, the O/I-Cu/ZnO catalyst displayed increased specific surface area, decreased Cu^0 particle size, and accordingly enhanced catalytic performance. If the amount of oxalic acid was excessive ($(COOH)_2$/(Cu+Zn) ratio>3.5/1), the catalyst particles would agglomerate and metal particles would sinter due to releasing a large amount of heat during the N_2 calcination process, resulting in decline of BET surface area of the catalyst and catalytic activity. Of all catalysts investigated, the O/I-Cu/ZnO catalyst obtained with $(COOH)_2$/(Cu+Zn) molar ratio of 3.5/1 exhibited best catalytic performance due to largest BET surface area and smallest Cu^0 particle size. Therefore, the $(COOH)_2$/(Cu+Zn) molar ratio of 3.5/1 was optimal for O/I-Cu/ZnO catalyst.

6-2. Influences of Calcination Conditions on Catalyst Performances

The influence of calcination temperature on catalyst performance was studied and the result is shown in Table S2. CO_2 conversion, and the selectivity and yield to methanol increased with increasing calcination temperature from 573 K to 623 K, and then decreased with further increasing the calcination temperature. The best catalytic performance was achieved on the catalyst calcined at 623 K. Note that although Cu^0 particle size was smaller, the obtained catalysts showed lower activity when the calcination temperature was lower than 623 K. This may be due to fewer Cu^0 active sites Cu^0 sites generated caused by incomplete decomposition of precursor and *in situ* reduction of CuO when the calcination temperature was low. The incomplete decomposition of precursor also resulted in lower BET surface area. At higher temperature, the Cu^0 size grew bigger and the surface area became smaller. Accordingly, the catalytic activity decreased. Therefore, the optimized calcination temperature was 623 K. The effect of heating rate of calcination on catalytic performance was also investigated. As shown in Table S3, the CO_2 conversion, and the selectivity and yield to methanol increased with increasing ramping rate from 1 $K \cdot min^{-1}$ to 3 $K \cdot min^{-1}$, and then decreased with increasing calcination heating rate from 3 $K \cdot min^{-1}$ to 5 $K \cdot min^{-1}$. The change rules of the specific surface area and Cu^0 particle size were consistent with that of the activity for O/I-Cu/ZnO catalyst. Best catalytic performance, largest specific surface area, and smallest Cu^0 particle size were achieved when the calcination heating rate was 3 $K \cdot min^{-1}$. At a slow ramping rate, the retention time of the catalyst at high temperature was too long, the chance of aggregation and sintering of metal Cu^0 increased. So, the specific surface area decreased and Cu^0 particle size increased at slower heating rate. When the calcination heating rate was too fast, the precursor decomposition reaction process was too violent, releasing a large amount of heat and reducing gas CO in a short period of time. Therefore, the BET surface area decreased and Cu^0 particle size increased due to catalyst particles aggregation and sintering of metal Cu^0. Besides, a part of the CO directly escaped from reaction system by the flow of N_2 before contacting CuO. As a result, CuO could not be completely reduced by the CO. When heating rate was appropriate (3 $K \cdot min^{-1}$), the precursor decomposition and CuO reduction process could proceed synergistically, and CuO could be fully reduced to Cu^0. Therefore, a ramping rate of 3 $K \cdot min^{-1}$ was used to prepare O/I-Cu/ZnO catalyst in this study.

The effect of calcination time on catalytic performance was also examined and the result is shown in Table S4. As the calcination time increased from 1 h to 3 h, the catalytic performance was enhanced. Further extending the holding time resulted in the decline of activity due to the increase of Cu^0 particle size. However, the precursor could not be decomposed completely when the calcination time was too short. Therefore, the appropriate calcination time was 3 hours.

6-3. Effect of Reduction Method on Catalyst Performance

To illustrate the advantage of *in situ* reduction, a control O/H-

Table 3. Effect of reduction method on catalyst performance[a]

Catalyst	CO_2 conversion/%	Selectivity/%		CH_3OH yield/%	S_{BET}[b]/$m^2 \cdot g$	d_{Cu}[c]/nm	S_{Cu}[d]/$m^2 \cdot g$
		CO	CH_3OH				
O/H-Cu/ZnO	27.54	23.14	76.86	21.17	32.87	25.9	3.2
O/I-Cu/ZnO	29.22	16.44	83.56	24.42	38.19	20.1	4.0

[a]Reaction conditions: 523 K; 3.0 MPa; catalyst weight: 0.5 g; $Ar/CO_2/H_2$=3/25/72; flowing rate: 18 $ml \cdot min^{-1}$; reaction time: 4 h
[b]BET specific surface area
[c]d_{Cu} determined by the XRD pattern based on Scherrer equation
[d]S_{Cu} determined from N_2O pulse chemisorption

Cu/ZnO catalyst obtained by conventional H_2 reduction was prepared. The Cu/Zn atomic ratio of O/H-Cu/ZnO is close to that of O/I-Cu/ZnO (Table S1). The catalytic performance of *in situ* reduced O/I-Cu/ZnO and H_2 reduced O/H-Cu/ZnO catalysts was comparatively studied, and the result is presented in Table 3. Compared with O/H-Cu/ZnO, O/I-Cu/ZnO catalyst exhibited higher CO_2 conversion, and the selectivity and yield to methanol. This could be explained by the fact that *in situ* reduction avoided additional H_2 reduction in high temperature, preventing the growth of active Cu^0 species and aggregation of catalyst particles, which was unavoidable during traditional H_2 reduction process, as confirmed by XRD (Fig. S1). Besides, the process was simple and solvent-free. Therefore, the *in situ* reduced O/I-Cu/ZnO catalyst prepared by oxalic acid assisted solid phase grinding method is a promising catalyst for the methanol synthesis reaction from CO_2 hydrogenation.

CONCLUSIONS

An oxalic acid assisted solid phase grinding method was employed to prepare Cu/ZnO catalyst for CO_2 hydrogenation to methanol. Copper and zinc oxalate complexes were obtained by grinding the mixture of the oxalic acid, copper nitrate and zinc nitrate at room temperature. The as-obtained precursor decomposed to CuO and ZnO, releasing reductive CO, and then CuO was subsequently reduced by CO to produce Cu^0 during calcination in N_2 needing no further H_2 reduction. It was found that the $(COOH)_2$/(Cu+Zn) molar ratio had a pronounced influence on physical-chemical properties of derived catalysts and corresponding catalytic performance. Appropriate oxalic acid dosage and calcination atmosphere could ensure the simultaneous precursor decomposition and CuO reduction. The smallest Cu^0 particle size and biggest specific surface area were achieved on catalyst with a $(COOH)_2$/(Cu+Zn) molar ratio of 3.5/1.0, which exhibited the highest catalytic performance. A series of calcination parameters were also systematically studied, such as calcination temperature, heating rate and holding time. The optimized calcination conditions were: temperature of 623 K, heating rate of 3 $K \cdot min^{-1}$ and holding time of 3 h. Compared with O/H-Cu/ZnO catalyst obtained by conventional H_2 reduction, *in situ* reduced O/I-Cu/ZnO catalyst exhibited larger specific surface area, smaller Cu^0 particle size and better catalytic performance. The avoiding of further high temperature H_2 reduction impeded the growth of active Cu^0 species and aggregation of catalyst particles was responsible for the excellent catalytic performance of O/I-Cu/ZnO catalyst.

ACKNOWLEDGEMENTS

The authors thank Prof. N. Tsubaki for fruitful discussions on the mechanism of CO_2 hydrogenation to methanol. The authors are grateful for the financial support from the National Natural Science Foundation of China (21528302, 51572272), Zhejiang Provincial Natural Science Foundation of China (LY14B030004), the Science and Technology Department of Zhejiang Province (2017C33007), the Scientific Research Foundation of the Education Department of Zhejiang Province (Y201635167), Open Foundation of Zhejiang Provincial Key Lab. for Chem. & Bio. Processing Technology of Farm Products, Zhejiang Provincial Collaborative Innovation Center of Agricultural Biological Resources Biochemical Manufacturing (2016KF0009, 2016KF0008) and the K.C. Wong Magna Fund in Ningbo University.

SUPPORTING INFORMATION

Additional information as noted in the text. This information is available via the Internet at http://www.springer.com/chemistry/journal/11814.

REFERENCES

1. D. Milani, R. Khalilpour, G. Zahedi and A. Abbas, *J. CO_2 Util.*, **10**, 12 (2015).
2. S. Saeidi, N. Amin and M. Rahimpour, *J. CO_2 Util.*, **5**, 66 (2014).
3. X. Jiang, N. Koizumi, X. Guo and C. Song, *Appl. Catal. B: Environ.*, **170**, 173 (2015).
4. X. Liang, X. Dong and G. Lin, *Appl. Catal. B: Environ.*, **88**, 315 (2009).
5. D. Wang, J. Zhao, H. Song and L. Chou, *J. Nat. Gas Chem.*, **20**, 629 (2011).
6. X. Dong, F. Li, N. Zhao, F. Xiao, J. Wan and Y. Tan, *Appl. Catal. B: Environ.*, **191**, 8 (2016).
7. I. Melián-Cabrera, M. Lopez Granados and J. Fierro, *J. Catal.*, **210**, 285 (2002).
8. L. Angelo, M. Girleanu, O. Ersen, C. Serra, K. Parkhomenko and A. Roger, *Catal. Today*, **270**, 59 (2016).
9. M. Pori, B. Likozar, M. Marinšek and Z. Crnjak Orel, *Fuel Process. Technol.*, **146**, 39 (2016).
10. S. Jadhav, P. Vaidya, B. Bhanage and J. Joshi, *Chem. Eng., Res. De.*, **92**, 2557 (2014).
11. X. Liu, G. Lu, Z. Yan and J. Beltramini, *Ind. Eng. Chem. Res.*, **42**,

6518 (2003).
12. J. Chen, W. Li and R. Shen, *Korean J. Chem. Eng.*, **33**, 500 (2016).
13. Y. Jeong, J. Kang, I. Kim, H. Jeong, J. Park, J. Park and J. Jung, *Korean J. Chem. Eng.*, **33**, 114 (2016).
14. L. Shi, P. Zhu, R. Yang, X. Zhang, J. Yao, F. Chen, X. Gao, P. Ai and N. Tsubaki, *Catal. Commun.*, **89**, 1 (2017).
15. X. Guo, D. Mao, G. Lu, S. Wang and G. Wu, *Catal. Commun.*, **12**, 1095 (2011).
16. J. Sun, L. Zhang, C. Ge, C. Tang and L. Dong, *Chinese J. Catal.*, **35**, 1347 (2014).
17. Q. Zhang, T. Zhang, Y. Shi, B. Zhao, M. Wang, Q. Liu, J. Wang, K. Long, Y. Duan and P. Ning, *J. CO_2 Util.*, **17**, 10 (2017).
18. P. Lu, C. Xing, H. Li, X. Gai, Q. Wei, L. Tan, C. Lu, W. Shen, R. Yang and N. Tsubaki, *Int. J. Hydrogen Energy*, **41**, 10680 (2016).
19. C. Tang, B. Sun, J. Sun, X. Hong, Y. Deng, F. Gao and L. Dong, *Catal. Today*, **281**, 575 (2017).
20. L. Wang, Y. Liu, M. Chen, Y. Cao, H. He, G. Wu, W. Dai and K. Fan, *J. Catal.*, **246**, 193 (2007).
21. I. Haq and F. Haider, *Mater. Lett.*, **63**, 2355 (2009).
22. D. Dollimore and D. Griffiths, *J. Therm. Anal.*, **2**, 229 (1970).
23. M. A. Gabal, *Thermochim. Acta*, **402**, 199 (2003).
24. D. Dollimore, D. Griffths and D. Nicholson, *J. Chem. Soc.*, **488**, 2617 (1963).
25. R. Yang, X. Yu, Y. Zhang, W. Li, N. Tsubaki, *Fuel*, **87**, 443 (2008).
26. J. Fei, Z. Hou, B. Zhu, H. Lou and X. Zheng, *Appl. Catal-A: Gen.*, **304**, 49 (2006).
27. L. Hong, R. Nie, G. Wu and Z. Hou, *Fuel*, **154**, 161 (2015).
28. D. Kim, C. Yang, Y. Park, K. Kim, S. Jeong, J. Han and Y. Lee, *Chem. Phys. Lett.*, **413**, 135 (2015).
29. J. Szanyi and D. Goodman, *Catal. Lett.*, **10**, 383 (1991).
30. R. van Santen, P. van Leeuwen, J. Moulijn and B. Averill, *Catalysis: An Integrated Approach*, **5**, 218 (1997).
31. K. Larmier, W.-C. Liao, S. Tada, E. Lam, R. Vérel, A. Bansode, A. Urakawa, A. Comas-Vives and C. Copéret, *Angew. Chem. Int. Ed.*, **56**, 2318 (2017).
32. G. Chinchen, K. Waugh and D. Whan, *Appl. Catal.*, **25**, 101 (1986).
33. P. Rasmussen, M. Kazuta and I. Chorkendorff, *Surf. Sci.*, **318**, 267 (1994).
34. P. Rasmussen, P. Holmblad, T. Askgaard, C. Ovesen, P. Stoltze, J. Nørskov and I. Chorkendorff, *Catal. Lett.*, **3-4**, 373 (1994).
35. J. Yoshihara and C. Campbell, *J. Catal.*, **2**, 776 (1996).
36. J. Yoshihara, S. Parker, A. Schafer and C. Campbell, *Catal. Lett.*, **4**, 313 (1995).
37. T. Fujitani, I. Nakamura, T. Watanabe, T. Uchijima and J. Nakamura, *Catal. Lett.*, **35**, 297 (1995).

Supporting Information

CO_2 hydrogenation to methanol over Cu/ZnO catalysts synthesized via a facile solid-phase grinding process using oxalic acid

Wenze Li*, Peng Lu*,†, Ding Xu***, and Kai Tao**,†**

*School of Applied Chemistry, Shenyang University of Chemical Technology, Shenyang 110142, China
**Department of Materials, School of Materials Science & Chemical Engineering,
Ningbo University, Ningbo, Zhejiang 315211, China
***School of Biological and Chemical Engineering, Zhejiang University of Science and Technology, Hangzhou 310023, China
(*Received 20 July 2017 • accepted 2 October 2017*)

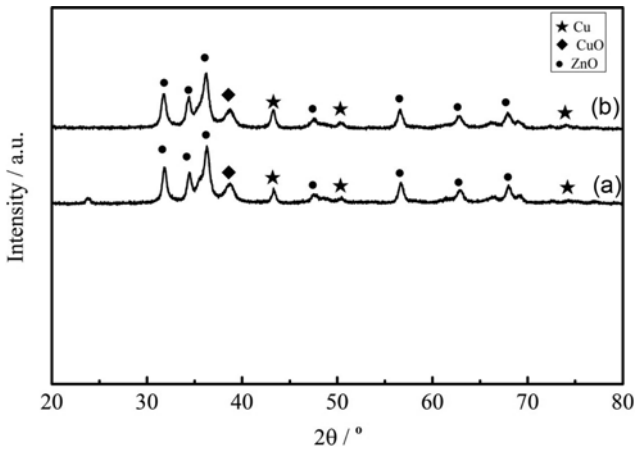

Fig. S1. XRD patterns of O/I-Cu/ZnO (a) and O/H-Cu/ZnO (b) catalyst.

Table S1. The EDS analysis of the as-prepared catalysts at various $(COOH)_2$/(Cu+Zn) molar ratios

Sample	Element content (atomic ratio)[a]			
	C	O	Cu	Zn
O/I-Cu/ZnO	20.38	15.21	35.56	28.85
O/H-Cu/ZnO	5.63	42.35	29.06	22.96

[a]Determined by EDX

Table S2. Influences of calcination temperature on catalytic performances

Calcination temperature/K	CO_2 conversion/%	Selectivity/%		CH_3OH yield/%	S_{BET}[a]/ $m^2 \cdot g$	d_{Cu}[b]/ nm
		CO	CH_3OH			
573	27.66	22.78	77.22	21.35	35.14	18.0
603	27.72	18.68	81.32	22.54	36.13	19.1
623	29.22	16.44	83.56	24.42	38.19	20.1
673	28.76	19.50	80.50	23.15	33.81	22.5

Reaction conditions: 523 K; 3.0 MPa; catalyst weight: 0.5 g; $Ar/CO_2/H_2$=3/25/72; flowing rate: 18 $ml \cdot min^{-1}$; reaction time: 4 h
[a]BET specific surface area
[b]d_{Cu} determined by the XRD pattern based on Scherrer equation

Table S3. Influences of calcination heating rate on catalyst performances

Heating rate/ $K \cdot min^{-1}$	CO_2 conversion/%	Selectivity/%		CH_3OH yield/%	$S_{BET}{}^a$/ $m^2 \cdot g$	$d_{Cu}{}^b$/ nm
		CO	CH_3OH			
1	27.54	22.64	77.36	21.30	32.54	23.1
2	28.56	24.72	75.28	21.50	36.07	20.8
3	29.22	16.44	83.56	24.42	38.19	20.1
4	28.38	23.12	76.88	21.82	35.04	21.4
5	27.36	23.58	76.42	20.91	29.77	23.4

Reaction conditions: 523 K; 3.0 MPa; catalyst weight: 0.5 g; $Ar/CO_2/H_2$=3/25/72; flowing rate: 18 $ml \cdot min^{-1}$; reaction time: 4 h

[a]BET specific surface area

[b]d_{Cu} determined by the XRD pattern based on Scherrer equation

Table S4. Influences of calcination time on catalyst performances

Calcination time/h	CO_2 conversion/%	Selectivity/%		CH_3OH yield/%	$S_{BET}{}^a$/ $m^2 \cdot g$	$d_{Cu}{}^b$/ nm
		CO	CH_3OH			
1	28.04	20.26	79.74	22.36	36.04	18.3
2	28.60	18.32	81.68	23.36	37.02	19.2
3	29.22	16.44	83.56	24.42	38.19	20.1
4	28.64	20.54	79.46	22.76	35.67	24.5

Reaction conditions: 523 K; 3.0 MPa; catalyst weight: 0.5 g; $Ar/CO_2/H_2$=3/25/72; flowing rate: 18 $ml \cdot min^{-1}$; reaction time: 4 h

[a]BET specific surface area

[b]d_{Cu} determined by the XRD pattern based on Scherrer equation